Title: Microstructure analysis of equiatomic multi-component ni20ti20ta20co20cu20 alloy

Author: Karsten Glowka, Maciej Zubko, Paweł Świec, Krystian Prusik, Grzegorz Dercz, Danuta Stróż

Citation style: Glowka Karsten, Zubko Maciej, Świec Paweł, Prusik Krystian, Dercz Grzegorz, Stróż Danuta. (2019). Microstructure analysis of equiatomic multi-component ni20ti20ta20co20cu20 alloy. "Archives of Metallurgy and Materials" (2019, iss. 2, s. 785-789), DOI: 10.24425/amm.2019.127614

Arch. Metall. Mater. **64** (2019), 2, 785-789

DOI: 10.24425/amm.2019.127614

K. GLOWKA*, M. ZUBKO*,**#, P. ŚWIEC*, K. PRUSIK*, G. DERCZ*, D. STRÓŻ*

MICROSTRUCTURE ANALYSIS OF EQUIATOMIC MULTI-COMPONENT $Ni_{20}Ti_{20}Ta_{20}Co_{20}Cu_{20}$ ALLOY

An equiatomic multi-component alloy $Ni_{20}Ti_{20}Ta_{20}Co_{20}Cu_{20}$ (at. %) was obtained using vacuum arc melting. In order to characterize such an alloy, microstructure analysis has been performed using Scanning and Transmission Electron Microscopy, Electron Backscattered Diffraction, X-ray Diffraction and Energy Dispersive X-ray Spectroscopy techniques. Microstructure analysis revealed the presence of one rhombohedral and two cubic phases. Energy Dispersive X-ray Spectroscopy measurements revealed that both observed phases include five chemical elements in the structure. Using Rietveld refinement approach the lattice parameters were refined for the observed phases.

Keywords: Thermodynamics, High Entropy Alloys, Multi-component alloys, electron microscopy, microstructure

1. Introduction

In recent years the group of multi-component alloys called high entropy alloys (HEAs) has been very popular and gained great attention of many research groups. The increased focus on this materials was started on the beginning of XXI century. First results obtained for multi-component alloys were published in 2004 by Cantor et al. [1]. Additionally, in the same year five more papers about high entropy alloys were published [2-6]. Based on chemical composition, high entropy alloys can be defined as alloys composed of at least five equimolar ratios or concentration of principal elements being between 5÷35 at. %. HEAs are also defined as alloys having configurational entropy at a random state equal to or greater than $1.5 \cdot R$ (where: R is a gas constant – 8.314 J/K · mol) [7]. Configurational entropy (ΔS_{conf}) can be calculated from following equation: $\Delta S_{conf} = -R\sum_{i=1}^{N} c_i \ln c_i$, where c_i is atomic fraction of element and R is gas constant. Configurational entropy also called mixing entropy (ΔS_{mix}) should be $\Delta S_{mix} \geq 13.39$ J/mol·K in the high entropy alloys [7]. The newest research of high entropy alloys showed that HEAs can have several interesting applications. Composition proposed by Lim et. al., i.e. Al-Co-Cr-Fe-Ni was thought as a material obtaining material for aerospace engine components [8]. Composition proposed by Hsu et. al., i.e. Cu-Co-Ni-Cr-Al-Fe [3] and modified by boron addition was studied to improve wear resistance and high temperature compression strength. Composition obtained by Senkov et. al., i.e. Al-Mo-Nb-Ta-Ti-Zr [9] was studied for refractory high entropy alloys.

The main goal of the present work was to obtain a new material that simultaneously meets the criteria of high-entropy alloys and exhibits shape memory effect. Ni and Ti were chosen as main elements for formation of Nitinol shape memory alloys [10]. The alloy additions such as Ta, Co and Cu also show a shape memory effect in various shape memory alloys [11-13]. High entropy alloys exhibiting shape memory effect are new group of high entropy materials and alloys of similar chemical composition have not been reported in the literature yet.

2. Materials and methods

Equiatomic $Ni_{20}Ti_{20}Ta_{20}Co_{20}Cu_{20}$ (at. %) alloy was obtained using vacuum arc melting in Ar protective gas atmosphere. Material was re-melted five times in order to obtain better homogeneity. Studied alloy was prepared from: nickel, titanium and copper pellets (a purity 99.999%), tantalum plates (a purity 99.999%) and cobalt lump (a purity 99.999%) commercially available.

Scanning Differential Calorimetry (DSC) measurements were performed using DSC equipment from Mettler Toledo company in the temperature range from –100 to 600°C with 10°C/min heating/cooling rate. Microstructure characterisation was performed on scanning electron microscope (SEM) JEOL JSM-6480 using the accelerating voltage of 20 kV equipped with the electron backscattered diffraction (EBSD) system manufactured by Oxford Instruments with Nordlys II detector and the Energy Dispersive X-ray Spectroscopy (EDS) detector from IXRF. Microstructure analysis was also carried out using

* UNIVERSITY OF SILESIA IN KATOWICE, INSTITUTE OF MATERIALS SCIENCE, 75 PUŁKU PIECHOTY 1A, 41-500 CHORZÓW, POLAND
** UNIVERSITY OF HRADEC KRÁLOVÉ, DEPARTMENT OF PHYSICS, HRADEC KRÁLOVÉ, CZECH REPUBLIC
# Corresponding author: maciej.zubko@us.edu.pl

JEOL JEM-3010 high-resolution transmission electron microscope (TEM) with 300 kV acceleration voltage, equipped with a Gatan 2k × 2k Orius™ 833 SC200D CCD camera. TEM thin foil sample with 3 mm diameter and ~100 μm thickness was grinded and Ar – ion polished on Gatan Precision Ion Polishing System (PIPS). Phase analysis based on X-ray powder diffraction (XRD) measurements was performed on a Panalytical Empyrean diffractometer with Cu anode ($Cu_{K\alpha}$ – λ = 1.54056 Å) working at an electric current of 30 mA, voltage of 40 kV and equipped with a PIXcell^{3D} detector. XRD phase analysis were performed using, reference standards from the International Centre for Diffraction Data (ICDD) PDF-4 database. Rietveld refinement was calculated using FullProf computer software [14]. TEM selected area electron diffraction (SAED) patterns were indexed using the ElDyf computer software.

3. Results

3.1. Thermodynamic description of the obtained material

The obtained alloy was characterized using Scanning Differential Calorimetry. DSC curves (Fig. 1).

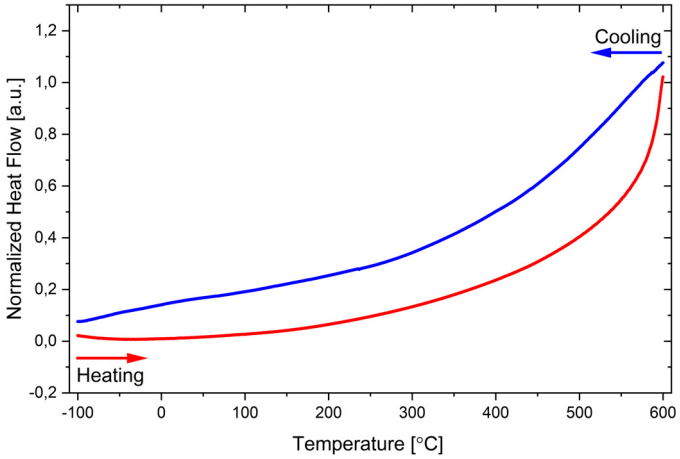

Fig. 1. DSC curves for studied alloy

The obtained DSC curves showed that the alloy does not exhibit any phase transformation and no shape memory effect occurs in the studied temperature range i.e. from –100 to 600°C.

An attention has been drawn on the formation mechanisms of solid solutions in high entropy alloys. The first supplementary parameter is atomic size mismatch – δ. The atomic size mismatch in case of HEAs should be in 0÷5% range [15]. Mismatch value above the critical range can suggest high level of crystal structure distortion. Chemical composition compatibility for many principal components is very often characterised by mixing enthalpy – ΔH_{mix} [16]. Mixing enthalpy (ΔH_{mix}) for HEAs should be in –15÷5 kJ/mol range [16-17]. Electronegativity differences parameter – $\Delta\chi$ is correlated with elemental segregation in alloys [11] and the formation of topologically close-packed (TCP) phases. For high entropy materials electronegativity should be in the range from –15 to 5 eV [18-20]. Last parameter is a valence electron concentration (VEC) which can suggest the formation of solid solution with *bcc* (VEC > 6.87) or *fcc* (VEC > 8.0) type of structure [19-20]. For solid solution forming there are supplementary parameters. First parameter proposed by Zhang et al. [21] is Ω defined as entropy of mixing multiplied the by average melting temperature of the elements over the enthalpy of mixing. The value $\Omega \geq 1$ should be chosen as critical value of solid solution forming in high entropy alloys. If the value Ω is less than 1, then there are predictions to form intermetallic compounds with some segregation. Next parameter proposed by Singh et. al. [22] is the Λ which describes the formation of disordered solid solutions (DSS) in high entropy alloys. Single DSSs are formed for the values of Λ above 0.96. For the range $0.24 < \Lambda < 0.96$, the mixture of two phases coexists and for the Λ value below 0.24 a mixture of compounds consisting of fcc bcc phases and precipitates is formed. The last parameter proposed by Wang et. al. [4] is the γ parameter which describes atomic packing misfit and topological instability. Critical value of atom misfit is $\gamma = 1.167$, which is correlated with Hume-Rothery rules about 15 % atomic size differences between elements in binary alloys. Solid solution forms for $\gamma \geq 1.167$, however the formation of multiphase regions with intermetallic phases along with metallic glasses was observed for $\gamma < 1.167$ [4]. These thermodynamics parameters described above are shown in Table 1 for the studied composition.

TABLE 1

Thermodynamics parameters for the studied alloy: atomic size mismatch – δ, mixing enthalpy – ΔH_{mix}, mixing entropy – ΔS_{mix}, electronegativity differences – $\Delta\chi$, valence electron concentration – VEC, entropy of mixing multiplied the by average melting temperature – Ω, disordered solid solutions (DSS) – Λ, atomic packing misfitting and topological instability – γ

δ [%] [15]	ΔH_{mix} [kJ/mol] [16]	ΔS_{mix} [J/mol·K] [7]	$\Delta\chi$ [eV] [20]	VEC [a.u.] [20]	Ω [21]	Λ [22]	γ [4]
6.92	–17.92	–13.38	0.19	7.80	1.51	0.27	1.00

All thermodynamic parameters predicted the formation of multi-phase solid solutions in the studied alloy.

3.2. Phase analysis using X-ray Diffraction

X-ray diffraction measurements for phase analysis were performed in the angular range of 2θ = 10÷110° with 0.02° steps (Fig. 2a).

Phase analysis using the PDF4+ ICDD (International Centre for Diffraction Data) database confirmed the presence of one rhombohedral and two cubic phases. First identified phase was the rhombohedral one with the crystal structure of the TaCo phase, lattice parameters a_0 = 4.9050 Å, c_0 = 26.3300 Å and space group $R\bar{3}m$ (PDF ICDD 04-003-6382). The second identified phase was the cubic one with structure similar to TiNi

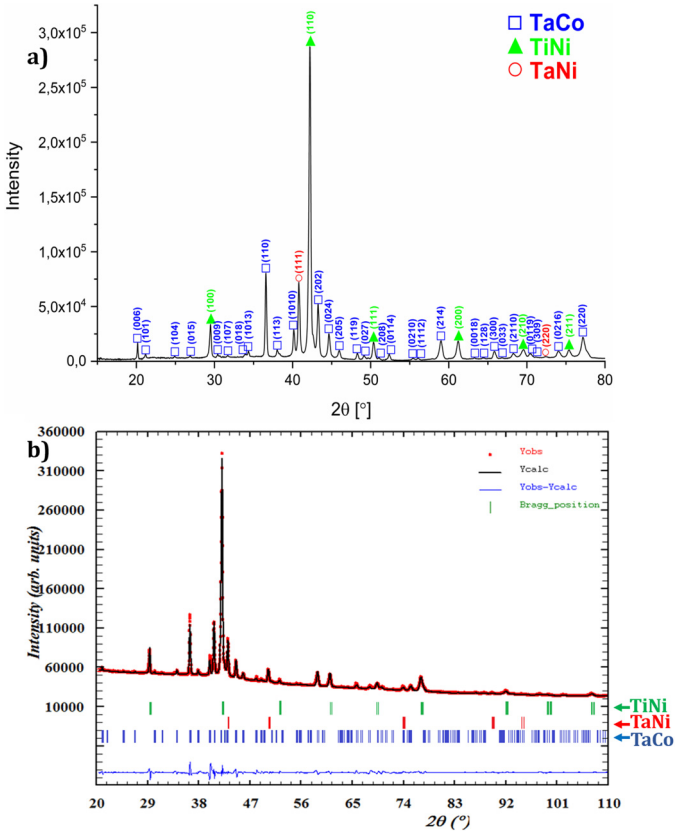

Fig. 2. a) X-ray diffraction pattern and b) X-ray diffraction pattern with residue profiles for studied alloy

with lattice parameter a_0 = 3.0250 Å and space group Pm$\bar{3}$m (PDF ICDD 04-015-0487). The last identified phase was also cubic one with the structure of TaNi phase with lattice parameter a_0 = 3.6230 Å and space group Fm$\bar{3}$m (PDF ICDD 04-001-0400). X-ray diffraction pattern shows that the strongest peak obtained for $2\theta = 26°$ representing {104} planes corresponds to the phase with structure similar to TaCo. Detailed analysis based on X-ray diffraction pattern (Fig. 2a) was performed using Rietveld method (Fig. 2b). For all phases Rietveld refinement revealed that lattice parameters are greater comparing to the ICDD data,

TABLE 2

Main parameters of phases from ICDD and after Rietveld refinement for studied alloy

Phase	TaCo	TiNi	TaNi
Crystal structure	Rhombohedral	Cubic	Cubic
Space group	R$\bar{3}$m	Pm$\bar{3}$m	Fm$\bar{3}$m
Lattice parameters from ICDD [Å]	a_0 = 4.9050 c_0 = 26.3300	a_0 = 3.0250	a_0 = 3.6230
ICDD	04-003-6382	04-015-0487	04-001-0400
Lattice parameters after Rietveld refinement [Å]	a_0 = 4.9265(3) c_0 = 26.5906(13)	a_0 = 3.0293(2)	a_0 = 3.6242(8)
Refined refined Volume [Å^3]	558.91(5)	27.80(1)	47.60(2)

which is related to implementing atoms with larger atomic radii into the original unit cells. For the phase similar to TaCo atomic radius of Ta (~1.430 Å) is bigger compared to the atomic radius of Co (~1.251 Å). For the phase similar to TiNi the atomic radius of Ti is larger than atomic radius of Ni. Atomic radii of these two elements are ~1.462 Å and ~1.246 Å for Ti and Ni, respectively. Additionally, for the phase similar to TaNi, unit cell expansion can be correlated with larger atomic radius of Ta.

3.3. Microstructure analysis

In order to perform microstructure analysis, Scanning Electron Microscopy (SEM) measurements were performed. SEM images revealed the presence of three different phases showing different composition contrast (Fig. 3). Such observations are in good agreement with the X-ray diffraction measurements confirming also the presence of three different phases.

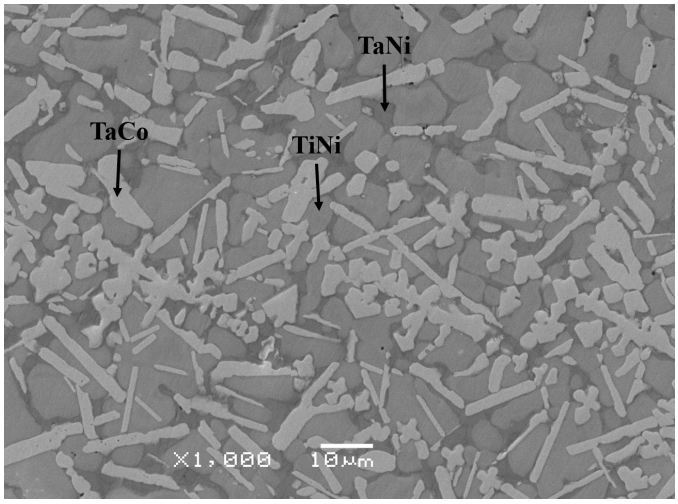

Fig. 3. SEM microstructure images with assigned phases for studied alloy

Electron Backscattered Diffraction technique confirmed also the presence of three phases which agrees well with phase and microstructure analysis. The obtained Kikuchi pattern allowed to assign an appropriate phase to the appropriate areas visible on the microstructure image showing different chemical contrast. The EBSD method confirmed the presence of phases similar to TaCo, TiNi and TaNi phases (Fig. 4).

An average chemical composition has been determined by use of Energy Dispersive X-Ray Spectroscopy technique for all three phases. The measurements showed that all phases contain all five principal chemical elements, however there are some variations depending on the phase. EDS measurements showed that the phase with the structure of TaCo is enriched in Ti, Co and Ta and depleted in Ni, Cu. The phase similar to TiNi is enriched in Ni, Ti, Co, Ta elements and depleted in Cu. The phase similar to TaNi phase is enriched in Ni, Co, Cu and depleted in Ti, Ta elements. Summary of average chemical compositions is shown in the Table 3.

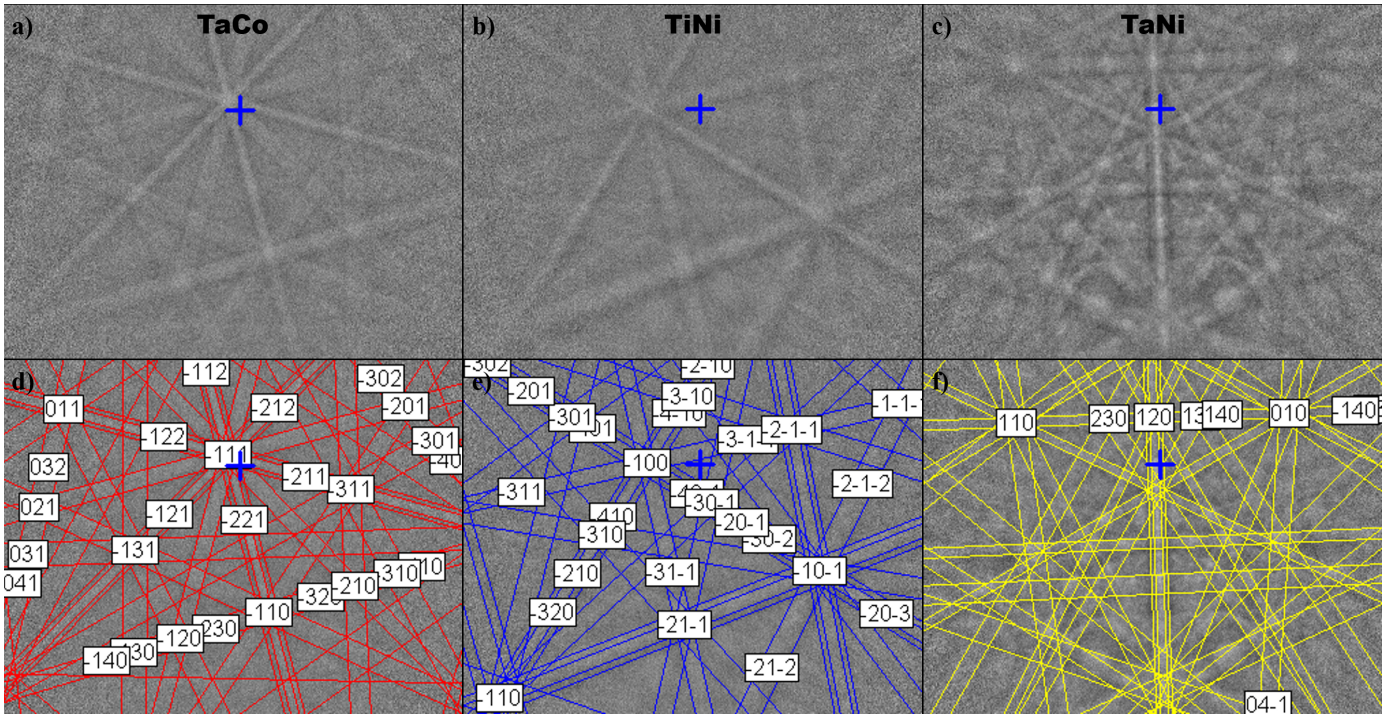

Fig. 4. Kikuchi lines and indexed patterns for (a-d) TaCo, (b-e) TiNi, (c-f) TaNi phases

Microstructure analysis was also performed use of TEM. Bright field images and corresponding selected area electron diffraction patterns were acquired and shown in Fig. 5.

TEM measurements confirmed the presence of the following phases i.e. TaCo, TiNi and TaNi. Bright field TEM microstructure image for the phase similar to TaCo (Fig. 5a)

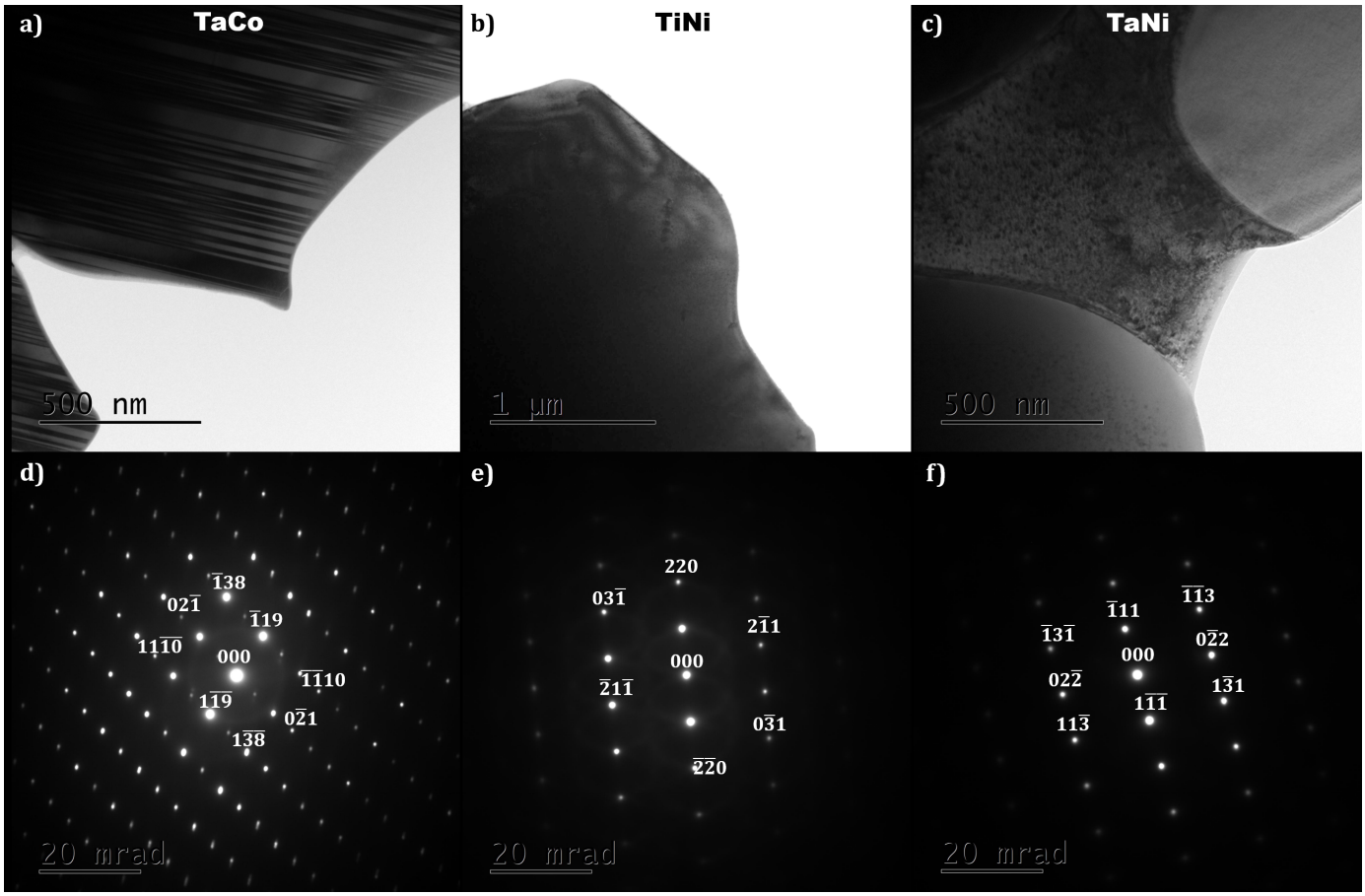

Fig. 5. Bright field and SAED images for (a-d) TaCo, (b-e) TiNi and (c-f) TaNi phases

TABLE 3

Average chemical composition of all phases

Phase	Elements and average at. %				
	Ti	Co	Ni	Cu	Ta
TaCo	8.6 (1.1)	22.2 (1.5)	15.4 (1.5)	7.8 (1.0)	45.9 (2.7)
TiNi	25.8 (0.7)	23.9 (0.9)	18.0 (0.9)	7.8 (2.3)	24.4 (1.2)
TaNi	16.3 (2.8)	5.3 (2.7)	17.4 (3.6)	53.4 (3.1)	7.4 (3.0)

revealed the presence of a lamellar structure. Such observations indicate presence of twin structure what is common for Cu enriched phases.

4. Conclusion

Equiatomic $Ni_{20}Ti_{20}Ta_{20}Co_{20}Cu_{20}$ (at. %) multi-component alloy was obtained by use of vacuum arc melting and consecutively re-melted five times. This kind of approach was applied for the first time. All the parameter's values foreseen formation of multi-phase alloy, which has been confirmed by all presented research methods. In the studied alloy no unreacted chemical elements was observed. XRD method revealed the presence of three phases with structures similar to: TaCo, TiNi and TaNi phases. Rietveld refinement revealed increasing values of lattice parameters for all these phases, which suggests the unit cell expansion caused by differences between atomic radii of elements. EBSD and SAED confirmed the presence of three phases. Chemical composition analysis using EDS method confirmed that all five principal elements exist in all three phases. Unfortunately, the studied NiTi-based alloy does not exhibit shape memory effect in the analysed temperature range. Further studies should be undertaken in order to investigate the influence of the mechanical treatment on the existence and character of the shape memory effect.

REFERENCES

[1] B. Cantor, I.T.H. Chang, P. Knight, A.J.B. Vincent, Mater. Sci. Eng. A, **375-377** (1-2), 213-218 (2004), DOI: https://doi.org/10.1016/j.msea.2003.10.257

[2] T.K. Chen, M.S. Wong, T.T. Shun, J.W. Yeh, Surf. Coatings Technol. **200** (5-6), 1361-1365 (2005), DOI: https://doi.org/10.1016/j.surfcoat.2004.08.023

[3] C.Y. Hsu, J.W. Yeh, S.K. Chen, T.T. Shun, Metal. Maters. Trans. A, **67** (7), 37-41 (2015), DOI: https://doi.org/10.1007/s11661-004-0254-x

[4] Z. Wang, Y. Huang, Y. Yang, J. Wang, C.T. Liu, Scr. Mater. **94**, 28-31, (2015), DOI: http://doi.org/10.1016/j.scriptamat.2014.09.010

[5] J.W. Yeh, S.K. Chen, J.Y. Gan, S.J. Lin, T.S. Chin, T.T. Shun, C.H. Tsau, S.Y. Chang, Metal. Maters. Trans. A **35** (8), 2533-2536 (2004), DOI: https://doi.org/10.1007/s11661-006-0234-4

[6] J.W. Yeh, S.K. Chen, S.J. Lin, J.Y. Gan, T.S. Chin, T.T. Shun, C.H. Tsau, S.Y. Chang, Adv. Eng. Mater. **6** (5), 299-303 (2004), DOI: https://doi.org/10.1002/adem.200300567

[7] M.C. Gao, C.S. Carney, N. Doğan, P.D. Jablonksi, J.A. Hawk, D.E. Alman. Jom. **67** (11), 2653-2669 (2015), DOI: https://doi.org/10.1007/s11837-015-1617-z

[8] K.R. Lim, K.S. Lee, J.S. Lee, J.Y. Kim, H.J. Chang, Y.S. Na, J. Alloys Compd. **728** (11), 1235-1238 (2017), DOI: https://doi.org/10.1016/j.jallcom.2017.09.089

[9] O.N. Senkov, J.K. Jensen, A.L. Pilchak, D.B. Miracle, H.L. Fraser, Mater. Des. **139**, 498-511 (2018), DOI: https://doi.org/10.1016/j.matdes.2017.11.033

[10] D. Stróż, G. Dercz, Z. Lekston, J. Rak, J. Palka, J. Pawlicki, Mater. Sci. Forum **674**, 53-60 (2011), DOI: https://doi.org/10.4028/www.scientific.net/MSF.674.53

[11] Z. Lekston, D. Stróż, M. Jędrusik-Pawłowska, Solid State Phenom. **163**, 118-122 (2010), DOI: https://doi.org/10.4028/www.scientific.net/SSP.163.118

[12] C.J. De Araújo, N.J. Da Silva, M.M. Da Silva, C.H. Gonzalez, Mater. Des. **32** (10), 4925-4930 (2011), DOI: https://doi.org/10.1016/j.matdes.2011.05.051

[13] J. Ma, F. Yang, J.I. Subirana, Z.J. Pu, K.H. Wu, Proc. SPIE **3324** (3), 50-57 (1998), DOI: https://doi.org/10.1117/12.316848

[14] J. Rodriguez-Carvajal, Physica B. **192** (1-2), 55-69 (1993), DOI: https://doi.org/10.1016/0921-4526(93)90108-I

[15] Y. Zhang, Y.J. Zhou, J.P. Lin, G.L. Chen, P.K. Liaw, Adv. Eng. Mater. **10** (6), 534-538 (2008), DOI: https://doi.org/10.1002/adem.200700240

[16] Y.F. Ye, Q. Wang, J. Lu, C.T. Liu, Y. Yang, Mater. Today **19** (6), 349-362 (2016), DOI: https://doi.org/10. 1016/j.mattod.2015.11.026

[17] A. Takeuchi, A. Inoue, Mater. Trans. **41** (11), 1372-1378 (2000), DOI: https://doi.org/10.2320/matertrans1989.41.1372

[18] Z.S. Nong, J.C. Zhu, Y. Cao, X.W. Yang, Z.H. Lai, Y. Liu, Mater. Sci. Technol. **30** (3), 363-369 (2014), DOI: https://doi.org/10.1179/1743284713Y.0000000368

[19] Y. Dong, Y. Lu, L. Jiang, T. Wang, T. Li, Intermetallics **52**, 105-109 (2014), DOI: https://doi.org/10.1016/j.intermet.2014.04.001

[20] S. Guo, C. Ng, J. Lu, C.T. Liu, J. Appl. Phys. **109** (10), 1-5, (2011), DOI: https://doi.org/10.1063/1.3587228

[21] X. Yang, Y. Zhang, Mater. Chem. Phys. **132** (3), 233-238 (2012), DOI: https://doi.org/10.1016/j.matchemphys.2011.11.021

[22] A.K. Singh, N. Kumar, A. Dwivedi, A. Subramaniam, Intermetallics **53** (5), 112-119 (2014), DOI: https://doi.org/10.1016/j.intermet.2014.04.019